論文 / 著書情報
Article / Book Information

Title	Design of Active Shield Circuit with Automatic Tuning Scheme
Authors	Retdian Agung NICODIMUS, Shigetaka Takagi
出典 / Citation	IEICE Transactions on Electronics, Vol. E88-C, No. 6, pp. 1196-1202
発行日 / Pub. date	2005, 6
URL	http://search.ieice.org/
権利情報 / Copyright	本著作物の著作権は電子情報通信学会に帰属します。 Copyright (c) 2005 Institute of Electronics, Information and Communication Engineers.

PAPER Special Section on Analog Circuit and Device Technologies

Nonlinear Analysis of Bipolar Harmonic Mixer for Direct Conversion Receivers*

Hiroshi TANIMOTO[†a)], ***Member***, **Ryuta ITO**[†], ***Student Member***, ***and*** **Takafumi YAMAJI**[††], ***Member***

SUMMARY An even-harmonic mixer using a bipolar differential pair (bipolar harmonic mixer;BHMIX) is theoretically analyzed from the direct conversion point of view; i.e, conversion gain, third-order input intercept point (IIP3), self-mixing induced dc offset level, and second-order input intercept point (IIP2). Also, noise are analyzed based on nonlinear large-signal model, and numerical results are given. Noises are treated as cyclostationary noises, thus all the folding effects are taken into account. Factors determining IIP3, IIP2, dc offset, and noise are identified and estimation procedures for these characteristics are obtained. For example, design guidelines for the optimal noise performance are given. Measured results support all the analysis results, and they are very useful in the practical BHMIX design.

key words: *harmonic mixer, BHMIX, theoretical analysis, down conversion mixer, conversion gain, IIP3, IIP2, self-mixing, dc offset, noise analysis, cyclostationary noise*

1. Introduction

The direct conversion receiver (DCR) architecture has been attracting much attention due to its capability to realize a single-chip solution for wireless transceivers. However, there are very difficult issues to overcome.

The most important issue is self-mixing which inevitably involves with conventional mixers [1]. This causes a huge time-varying dc output, which is very difficult to remove once produced. Another issue may be a required very large IIP2, in addition to an IIP3, which is of the primary concern in conventional mixers. The reason for required large IIP2 is that any spectra input from an RF port of the mixer falls into dc by the second-order nonlinearity of the mixer and possibly corrupts the down-converted signals.

Even-harmonic type of mixers (EHMIX) play a unique role in the DCR architecture, because they have no dc offset fluctuations, in principle, caused by the self-mixing process, and have very large IIP2 due to its inherent odd-symmetric device characteristic. Thus in addition to IIP3, major design concerns for the EHMIX include the way imperfection in odd-symmetry affects the important characteristics for DCR mixers such as conversion gain, output dc offset, and input intercept points.

Manuscript received November 11, 2004.
Manuscript revised January 9, 2005.

[†]The authors are with the Dept. of Electrical and Electronic Eng., Kitami Institute of Technology, Kitami-shi, 090-8507 Japan.
[††]The author is with the Corporate R & D Center, Toshiba Corp., Kawasaki-shi, 212-8582 Japan.

*Preliminary versions of this work were presented at MWE 2001 [5] and MWSCAS 2004 [7].

a) E-mail: tanimoto@elec.kitami-it.ac.jp

DOI: 10.1093/ietele/e88–c.6.1203

A bipolar harmonic mixer (BHMIX) is a kind of EHMIX, which uses a bipolar differential pair as a harmonic mixer core [2], [3]. Fundamental characteristics of the BHMIX have been investigated mainly through experiments [2], [3], and is used for cellular telephone receivers [4]; however, there have been few papers which theoretically treat the BHMIX's important characteristics like conversion gain, IIP3, IIP2, dc offset [5], and signal-to-noise ratio (SNR) or noise figure (NF) etc. [6], [7].

In this paper, we first present nonlinear analyses of BHMIX for conversion gain, IIP3, IIP2 due to offset of bipolar differential pair. Next, we present a complete noise analysis of BHMIX considering both thermal noise of base resistances and collector shot noises with an assumption of static hypertangent input/output transfer characteristic for the bipolar differential pair. Results of the analysis are compared with measured results will then be given. Finally come concluding remarks.

2. Nonlinear Large-Signal Analysis of BHMIX

The nonlinear device used in the EHMIX may be a two-terminal device, a three-terminal device, or whatever device with odd symmetry. Historically, an anti-parallel diode pair (APDP) has been exclusively used to date [8], [9]. However, we need to separate local oscillator (LO), radio frequency (RF), and output baseband signals by using complicated filters [9], because the APDP is a two-terminal device and hence, these three signals coexist on the same port.

The authors introduced an EHMIX based on a BJT differential pair, which is a three-terminal device (Fig. 1) [2]. A differential pair has two input terminals and an output port. This naturally fits a mixer's functionality and can take advantage of removal for complicated signal separation filters. In addition, we can expect a conversion *gain* instead of con-

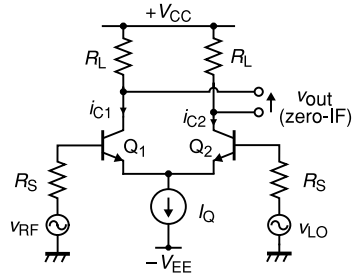

Fig. 1 EHMIX based on a BJT differential pair.

version loss as in the APDP case, because this is an active mixer.

Now, let us consider a static nonlinear input-output relation:

$$y = a_0 + a_1 x + a_2 x^2 + a_3 x^3 + \dots \tag{1}$$

where x is an input and y is an output quantity, and a_k ($k = 0, 1, 2, 3, \dots$) are coefficients for each power of x. It should be noted that the output frequency is different from input frequency in a mixer case. Thus the coefficient a_1 is a usual conversion gain for a mixer.

The second (third) order input intercept point IIP2 (IIP3) is defined as an input value at which the output components due to x term and x^2 (x^3) term become equal, and are calculated by the following formulas [10]:

$$\text{IIP2} = |a_1/a_2|, \quad \text{IIP3} = \sqrt{|4a_1/3a_3|} \tag{2}$$

The transfer characteristic of the differential pair is described by the following equation:

$$i_{\text{out}}(t) \equiv i_{\text{C1}}(t) - i_{\text{C2}}(t) = \alpha_{\text{F}} I_{\text{Q}} \tanh\left\{\frac{v_{\text{diff}}(t)}{2V_{\text{T}}}\right\}, \tag{3}$$

where, the symbols are defined as follows. i_{out}: a differential output current of the differential pair, $\alpha_{\text{F}} \approx 1$: a forward current gain of the transistors, I_{Q}: the tail current, v_{diff}: a differential input voltage across the base terminals, V_T: the thermal voltage. Here an LO drive for the BHMIX is $v_{\text{LO}}(t) = V_{\text{LO}} \cos \omega_{\text{LO}} t$, and an RF signal is $v_{\text{RF}}(t) = V_{\text{RF}} \cos \omega_{\text{RF}} t$; i.e, $v_{\text{diff}}(t) = v_{\text{LO}}(t) - v_{\text{RF}}(t)$. We assume that $\omega_{\text{RF}} = 2\omega_{\text{LO}}$ holds, and introduce normalized variables $y \equiv v_{\text{out}}/(\alpha_{\text{F}} I_{\text{Q}})$ and $x \equiv v_{\text{diff}}/2V_{\text{T}}$ to simplify the analysis. We neglect source resistances R_{S} except for noise analysis, because the input impedance of the differential pair is much larger than R_{S} in most practical cases.

We first calculate small signal conversion gain for desired output and third order intermodulation (IM3) output.

Let normalized large signal LO drive be $\alpha \cos\theta$, and δ be the small input signal. As we are interested in the direct conversion receiver, the input signal is assumed to be $\delta = \beta \cos 2\theta$; i.e, the output becomes dc voltage. A normalized output dc voltage of the BHMIX can be calculated by averaging $y(\theta)$ over a period of 2π, as a function of α and β.

The output is given by (4) and its power series expansion in terms of δ becomes (5):

$$y = \tanh(\alpha \cos\theta + \delta) \tag{4}$$

$$= f_0(\alpha \cos\theta) + f_1(\alpha \cos\theta)\,\delta + f_2(\alpha \cos\theta)\,\delta^2 + f_3(\alpha \cos\theta)\,\delta^3 + o(\delta^4), \tag{5}$$

where $f_i(\cdot)$ $(i = 0, 1, 2, 3)$ are given by:

$$f_0(x) \equiv \tanh x, \tag{6}$$

$$f_1(x) \equiv 1 - \tanh^2 x, \tag{7}$$

$$f_2(x) \equiv -\tanh x\,(1 - \tanh^2 x), \tag{8}$$

$$f_3(x) \equiv -(1 - \tanh^2 x)\,(1 - 3\tanh^2 x). \tag{9}$$

These coefficients have following implications:

0th degree coefficient f_0: Output component that is nothing to do with input δ, i.e, LO leakage component.

1st degree coefficient f_1: Output component that is proportional to δ. This term is a periodic even function of θ and can be expanded into a Fourier series which consists of only even order Fourier coefficients. Its second harmonic Fourier coefficient is proportional to the conversion gain. If the frequency of δ is $2f_{\text{LO}}$ as with usual direct conversion receiver case, the desired output is found at zero frequency, i.e, at dc.

2nd degree coefficient f_2: Output component that is proportional to the second order distortion of δ. Because the 2nd degree coefficient is a periodic odd function of θ, no dc output will be produced if the frequency of δ is twice the LO frequency as in the case of direct conversion receiver, i.e, $\delta = \beta \cos 2\theta$. Thus these components do not exist in our direct conversion case and can be neglected. However, if the input contains a dc component, γ, the input becomes $\delta = \beta \cos 2\theta + \gamma$ and the output dc component will be produced. This is the mechanism of IM2, which will be analyzed later.

3rd degree coefficient f_3: Output component that is proportional to the third order distortion of δ. This term is an even function and can be expanded into a Fourier series with only odd harmonics of f_{LO}. If the frequency of δ is $2f_{\text{LO}}$, the output frequencies are $2nf_{\text{LO}} \pm 2f_{\text{LO}}$, and these are even harmonics of f_{LO}. As we are interested in the third order intermodulation distortion, and from the trigonometric identity $\cos^3 x = (3/4)\cos 2x + (1/4)\cos 6x$, we see input frequencies from $2f_{\text{LO}}$ and $6f_{\text{LO}}$ can produce dc component, which is indistinguishable from desired output. This is the IM3 component.

2.1 Conversion Gain

From the above discussion, we can calculate the down converted output dc component I_1 for a small signal of $\delta = \beta \cos 2\theta$:

$$I_1 = \frac{1}{2\pi} \int_0^{2\pi} f_1(\alpha \cos\theta)\,\beta \cos 2\theta \, \mathrm{d}\theta. \tag{10}$$

Thus we have the small signal conversion gain formula:

$$\eta = \left.\frac{\mathrm{d}I_1}{\mathrm{d}\beta}\right|_{\beta \to 0} = \frac{1}{2\pi} \int_0^{2\pi} \{1 - \tanh^2(\alpha \cos\theta)\} \cos 2\theta \, \mathrm{d}\theta \equiv a_1 \tag{11}$$

Figure 2 shows the numerically calculated magnitude of normalized conversion gain $|\eta|$ vs. normalized LO signal amplitude α. This small signal conversion gain has a broad peak and reaches its maximum at $\alpha \approx 1.93 = 100.3\,\text{mV}$. This corresponds to $-9.97\,\text{dBm}$ when the LO signal is fed to a fictitious $50\,\Omega$ load. Conversion gain variation due to LO-amplitude variation can be minimized by setting it around $100\,\text{mV}$.

Note that the conversion gain rises in proportion to the

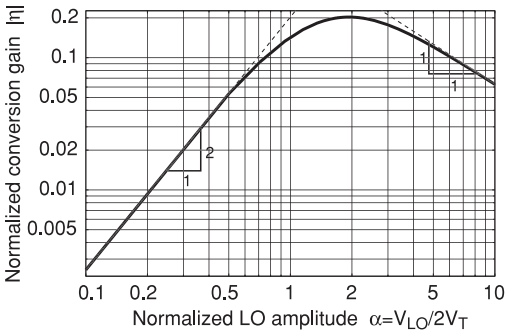

Fig. 2 Conversion gain vs. LO amplitude (BJT differential pair).

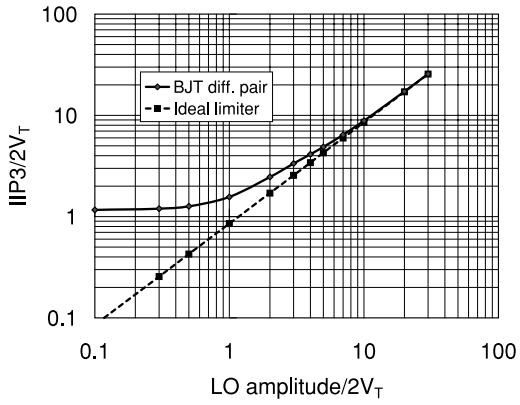

Fig. 3 Normalized IIP3 characteristics (BJT differential pair).

square of α in a region $\alpha < 1$, while it falls in proportion to $1/\alpha$ for a region $\alpha > 3$. The square-law dependence of the conversion gain implies that the output comes from a third-order modulation product; i. e, $f_{\text{out}} = 2f_{\text{LO}} - f_{\text{RF}}$. On the other hand, the reciprocal dependence is due to a limiter type nonlinearity which can be interpreted by the PWM model [2], [5].

2.2 Third Order Intercept Point

Likewise, the dc output components due to the third order intermodulation distortion can be calculated as the conversion gain case. Let the second harmonic Fourier cosine coefficient be c_{32} and the 6th harmonic Fourier cosine component be c_{36}:

$$c_{32} \equiv \frac{1}{2\pi}\int_0^{2\pi} f_3(\alpha\cos\theta)\,\cos 2\theta\,\mathrm{d}\theta, \tag{12}$$

$$c_{36} \equiv \frac{1}{2\pi}\int_0^{2\pi} f_3(\alpha\cos\theta)\,\cos 6\theta\,\mathrm{d}\theta. \tag{13}$$

Thus for a small input $\delta = \beta\cos 2\theta$, we have a dc output I_3 due to IM3:

$$I_3 = \left[\frac{3}{4}c_{32} + \frac{1}{4}c_{36}\right]\beta^3 \equiv a_3\beta^3 \tag{14}$$

Hence we have $a_3 = 3c_{32}/4 + c_{36}/4$. Putting (11) and (14) into (2), the IIP3 can be obtained by

$$\text{IIP3} = \sqrt{\frac{4}{3}\left|\frac{a_1}{a_3}\right|} = \sqrt{\frac{4}{3}\left|\frac{a_1}{3c_{32}/4 + c_{36}/4}\right|}. \tag{15}$$

A numerically calculated α vs. IIP3 curve of the BHMIX is plotted in Fig. 3, along with IIP3 curve of an ideal limiter [5]. The differential pair curve approaches the limiter curve for large values of LO amplitude.

2.3 Self Mixing and Second Order Intercept Point

A BJT differential pair inevitably has an input dc offset voltage, $\delta = \gamma$, due to imperfect matching and processing variations. This offset causes an errornous dc output. As the offset γ usually is very small compared with the LO signal amplitude, the offset behaves just like a small signal RF input signal except its polarity [5]. Thus the output dc current due to self-mixing is given by

$$I_{\text{self-mixing}} = \frac{1}{2\pi}\int_0^{2\pi} f_2(\alpha\cos\theta)\,\gamma\,\mathrm{d}\theta. \tag{16}$$

This poses an extraordinarily stringent requirement for the differential pair's offset, because the RF input signal can be as small as tens of micro volts. However, the input offset, γ, is very small in any way, and may follow the superposition law along with RF input signals. In addition, a static offset cancellation scheme may be effective as the offset does not change rapidly [11].

If an RF input, $\beta\cos 2\theta$, coexists with the offset, γ, it also invokes second-order intermodulation (IM2) by introducing nonzero a_2 term.

For small γ, the second order coefficient of δ in (5) can be approximated as follows:

$$f_2(\alpha\cos\theta + \gamma) \approx f_2(\alpha\cos\theta) + f_2'(\alpha\cos\theta)\,\gamma, \tag{17}$$

$$\text{with}\quad f_2'(x) = 1 - 4\tanh^2 x + 3\tanh^4 x. \tag{18}$$

Then, the output dc current due to second order distortion, I_2, is given by:

$$I_2 \approx \frac{1}{2\pi}\int_0^{2\pi} f_2'(\alpha\cos\theta)\,\gamma(\beta\cos 2\theta)^2\,\mathrm{d}\theta \equiv a_2\beta^2, \tag{19}$$

$$\text{or,}\quad a_2 = \frac{\gamma}{2\pi}\int_0^{2\pi} f_2'(\alpha\cos\theta)\,\cos^2 2\theta\,\mathrm{d}\theta. \tag{20}$$

Now we can calculate IIP2 with the above a_2 and a_1 from (11) by using (2). That is,

$$\text{IIP2} = \left|\frac{a_1}{a_2}\right| = \left|\frac{\int_0^{2\pi} f_1(\alpha\cos\theta)\,\cos 2\theta\,\mathrm{d}\theta}{\gamma\int_0^{2\pi} f_2'(\alpha\cos\theta)\,\cos^2 2\theta\,\mathrm{d}\theta}\right|. \tag{21}$$

In Fig. 4, numerically calculated IIP2 curves for several LO amplitudes are plotted to the offset γ. IIP2 is referred to RF input, thus measures just the same as β.

The lines run in parallel, but do not obey the "α^2 law"

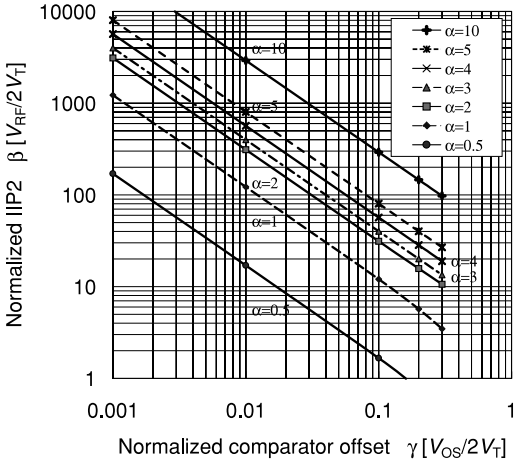

Fig. 4 IIP2 vs. differential pair offset. Normalized LO amplitude, α, is taken as a parameter.

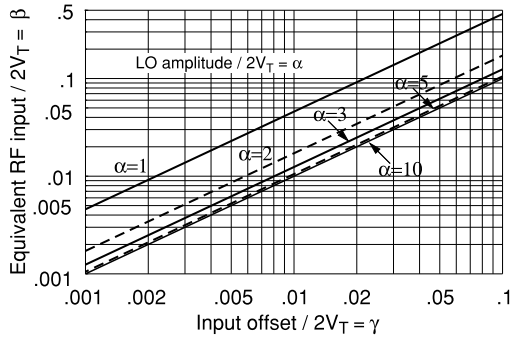

Fig. 5 Equivalent RF input level vs. input offset. Normalized LO amplitude α is taken as a parameter.

unlike an ideal limiter case [5]. This is because the nonlinearity of the differential pair is represented by a hypertangent function. When the α value becomes larger, the tanh function behaves like the ideal limiter; in fact, $\alpha = 5$ and $\alpha = 10$ lines run in parallel, about 4 times apart each other, as predicted from the limiter case.

In any case, we can predict IIP2 for a given input offset of the differential pair V_{OS} using this result; for example, if $V_{OS} = 0.52$ mV and the LO amplitude $V_{LO} = 104$ mV, i.e, $\gamma = 0.01$ and $\alpha = 2$, we obtain IIP2 $= 312 \times 2V_T \approx 16.2$ V. This corresponds to an IIP2 of 34.2 dBm when the circuit impedance is 50 Ω. This is not very high but a modest performance. This can be further improved by introducing a balanced structure [3], [4].

For an offset-induced self-mixing, Fig. 5 shows relation between equivalent RF input level, β, which causes the same amount of output dc component and differential pair input offset, γ, with LO signal amplitude, α, as a parameter. The lines are numerically calculated in a similar way as in the case of IIP2 with the RF-signal level kept zero ($\beta = 0$). The lines approach a $\beta = \gamma$ line as α becomes large. A large α implies an ideal limiter, so that the input referred dc offset β must coincide with γ, the input dc of the limiter itself. This is quite a reasonable consequence if one would use a limiter with an offset. The input offset V_{OS} changes very slowly and does not change much in practice, and a static offset cancellation can be effective.

For a numerical example, $\gamma = 0.01$ ($V_{OS} = 0.52$ mV) and $\alpha = 3$ ($V_{LO} = 156$ mV) yields an equivalent RF-input level of $\beta \approx 0.0127$ ($V_{RF} \approx 0.66$ mV), i.e, −54 dBm at a fictitious 50 Ω load. The dc offset value seems too large; however, this means that if another 156 mV was added to the RF port, the input-referred offset would have increased by 0.66 mV. Thus to achieve the change in offset level of −100 dBm, for example, we need to expect an isolation of 46 dB from LO to RF port. This is not an easy level of isolation at GHz range with the current Si-LSI technology; however, it may be made possible by introducing a balanced structure [2].

3. Noise Analysis of BHMIX

In the noise analysis of a mixer, we have to consider time varying nature of the output noises, unlike linear circuits as LNA etc., because the mixer is a nonlinear time-varying circuit. This means that the output noises are nonstationary, and we cannot directly make use of familiar linear noise analysis techniques. However, the noise sources are so small compared with the periodic LO drive signal that we can model the mixer as a linear periodically time varying (LPTV) circuit [12]. In addition, both thermal noise and shot noise outputs are modeled by periodically modulated stationary noises, i.e, cyclostationary noises [12].

The output signal v_{out} in Fig. 1 contains several major noise contributions; i. e, thermal noise from base resistances, r_b, collector shot noises of Q_1 and Q_2, and the noise from the tail current I_Q. Thermal noises of the load resistors R_L, base shot noises of Q_1 and Q_2 are less significant and are ignored for simplicity.

The equivalent input thermal noise voltage of r_b at the base terminal in Fig. 1 is constant; however, corresponding output noise can be modeled as a modulated version of the input thermal noise, because the gain of the differential amplifier periodically changes with the LO drive signal.

The collector shot noise produced by a constant bias current is a stationary white noise. For the BHMIX case, in contrast, the collector bias current is not constant but varies with the LO drive signal. Assuming that the noise generating mechanisms are very much faster than the LO drive frequency, we can model the output noise by an amplitude modulated white noise [12], [13]. Hence the collector shot noise may also be modeled by an amplitude modulated stationary white noise with time varying envelope in our case.

As the output noises are small, we can calculate the noise outputs from small-signal equivalent circuit shown in Fig. 6 as usual; however, the small signal quantities in Fig. 6 are not constant, because Q_1 and Q_2 are nonlinear devices and their operating points are periodically changing with time by the differential input voltage:

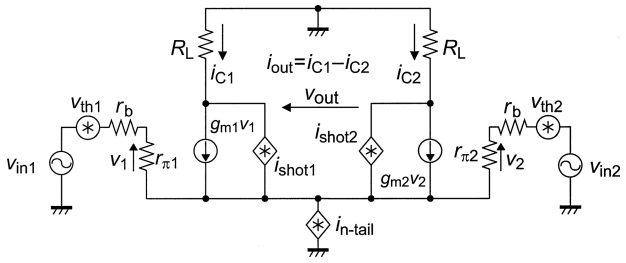

Fig. 6 Small-signal equivalent circuit for BHMIX.

$$\begin{cases} i_{C1}(t) = \dfrac{\alpha_F I_Q}{2}\left(1 - \tanh\dfrac{v_{LO}(t) - v_{RF}(t)}{2V_T}\right) \\ i_{C2}(t) = \dfrac{\alpha_F I_Q}{2}\left(1 + \tanh\dfrac{v_{LO}(t) - v_{RF}(t)}{2V_T}\right) \end{cases} \tag{22}$$

where $\alpha_F \approx 1$ is a forward current gain of a common base transistor, and $V_T = kT/q$ is the thermal voltage. Using those collector current values with $v_{RF} = 0$, transconductances and input impedances are obtained by

$$g_{mk} = i_{Ck}/V_T, \quad r_{\pi k} = \beta_F/g_{mk}, \quad (k = 1, 2), \tag{23}$$

where $\beta_F \gg 1$ is a forward current gain of a common emitter transistor.

3.1 Noise Spectrum of Amplitude Modulated White Noise

An amplitude modulated white noise $n(t)$ can be modeled by

$$n(t) = a(t)w(t), \tag{24}$$

where $a(t)$ is a T-periodic modulating function, i.e. envelope, and $w(t)$ is a stationary white noise. Such $n(t)$ becomes a cyclostationary process with a period T [13].

A measured power spectrum density of the above $n(t)$ can be represented as a following expression:

$$S_0(\omega) \approx \sigma^2 \sum_{n=-\infty}^{+\infty} |c_n|^2, \tag{25}$$

where σ^2 is a power spectrum density of $w(t)$, and c_n is an n-th Fourier coefficient of $a(t)$. See Appendix for its derivation.

It should be noted that (25) includes all the folding noise contributions to the baseband from harmonics of the LO fundamental frequency, since $a(t)$ is determined by a particular LO wave form like sinusoid, triangle etc. We will calculate c_n for sinusoidal LO case in section 3.5. The process accumulating all the foldings by (25) is similar what was done intuitively for normal mixers in [14]; however, the reference [14] assumed all the noises to be stationary.

Assuming that the shot noise and thermal noise are very small compared with the LO signal, and have no correlation with each other, we can calculate the total output noise by simply adding them as rms values. Before doing this, we must calculate their envelopes next.

3.2 Output Shot Noise Envelope

In Fig. 6, $i_{\text{shot}\,k} = \sqrt{2qi_{Ck}}$, $(k = 1, 2)$ are collector shot noise sources. We calculate them as a function of x and I_Q, as they change with instantaneous LO drive $v_{LO}(t)$.

The output noise component of the shot noise is obtained by solving the nodal equation for Fig. 6 with $v_{in1} = v_{LO}$ and $v_{in2} = 0$ [7]:

$$\overline{i^2_{\text{shot}}} = \frac{qI_Q \operatorname{sech}^2 \frac{v_{LO}}{2V_T}\left(1 + \cosh\frac{v_{LO}}{V_T} + 4\beta_F + 2\beta_F^2\right)}{(1+\beta_F)^2} \tag{26}$$

$$\approx 2qI_Q \operatorname{sech}^2 \frac{v_{LO}(t)}{2V_T} \quad (\beta_F \gg 1) \tag{27}$$

where q is a charge of an electron, and V_T is the thermal voltage. Equation (26) indicates that the output shot noise amplitude is an even function of $v_{LO}(t)$.

3.3 Output Thermal Noise Envelope

We consider thermal noise of only base resistance r_b for simplicity. Put equivalent thermal noise generators v_{th1} and v_{th2} in series with base terminals, then neglect r_b. This is because $r_b \ll r_\pi$ holds in most cases. v_{th1} and v_{th2} have rms voltage of $\sqrt{4kTr_b}$ each at the input. In order to compare contribution of thermal noise with that of shot noise, thermal noise needs to be referred to output current i_{thermal}.

Small signal transconductance g_m, at the operating point, from v_{in1} is given by

$$g_m \approx \frac{d}{dv_{LO}} I_Q \tanh\left(\frac{v_{LO}}{2V_T}\right) = \frac{I_Q}{2V_T}\operatorname{sech}^2\left(\frac{v_{LO}(t)}{2V_T}\right). \tag{28}$$

Here α_F is assumed to be unity and is dropped. Now the output mean square thermal noise is given by [7]:

$$\overline{i^2_{\text{thermal}}} = 4kT \cdot 2r_b \times {g_m}^2 = \frac{2qr_b}{V_T} I_Q^2 \operatorname{sec}^4\left(\frac{v_{LO}(t)}{2V_T}\right). \tag{29}$$

This also is an even function of $v_{LO}(t)$.

Comparing (29) with (26), we notice that while shot noise $\overline{i^2_{\text{shot}}}$ is proportional to I_Q, thermal noise $\overline{i^2_{\text{thermal}}}$ is proportional to I_Q^2. This indicates that the thermal noise dominates over the shot noise as I_Q becomes larger.

Figure 7 shows an example of the relation between output noise power density and static LO drive voltage v_{LO}.

3.4 Output Noise Due to Tail Current Noise

Next, we estimate a noise contribution from the tail current. As indicated in Fig. 6, we assume that a noise current source i_{n-tail} exists in parallel with the tail current source I_Q of Fig. 1.

The differential output noise current component due to i_{n-tail} can simply be calculated by (3)

$$i_{out}(t) = \alpha_F i_{n-tail} \tanh\{v_{LO}(t)/2V_T\}. \tag{30}$$

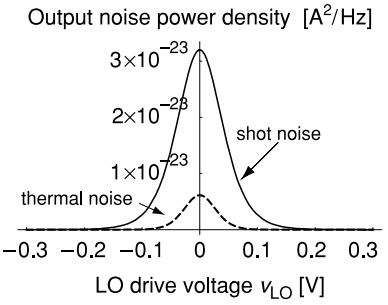

Fig. 7 Output noise power density vs. instantaneous LO drive voltage. Calculated for $I_Q = 0.1$ mA, and $r_b = 50\,\Omega$, $V_{LO} = 50$ mV.

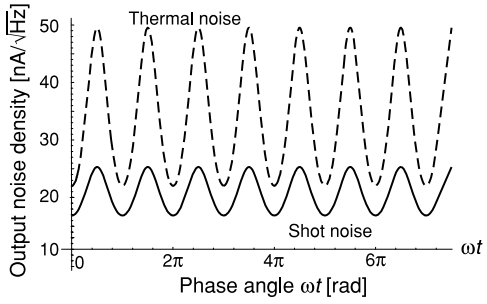

Fig. 8 Envelopes of modulated shot noise and thermal noise. Calculated for $I_Q = 2$ mA, and $r_b = 50\,\Omega$, $V_{LO} = 50$ mV.

Then the mean square envelope of the output noise current due to the tail current noise can be obtained by

$$\overline{i_{out}^2} \approx \overline{i_{n-tail}^2} \tanh^2 \{v_{LO}(t)/2V_T\}. \tag{31}$$

As $\overline{i_{n-tail}^2}$ is constant, this implies that $\overline{i_{out}^2}$ is an even function of LO drive voltage, and if $|v_{LO}(t)| \ll V_T$, $\overline{i_{out}^2} \simeq 0$ holds, and if $|v_{LO}(t)| \gtrsim 2V_T$, $\overline{i_{out}^2} \simeq \overline{i_{n-tail}^2}$ holds. Thus a larger LO drive results in a larger output noise, but it rapidly saturates for $|v_{LO}(t)| \gtrsim 2V_T$. This noise component could have a significant contribution to the total noise; however, we will not discuss it further because introducing a simple emitter degeneration resistor, R_E, in the tail current source can reduce i_{n-tail} by an amount of local feedback loop gain ($1 + g_m R_E \gg 1$) so that its contribution can be made negligible among other noise sources.

3.5 Output Noise as a Function of LO Amplitude

Figure 8 shows examples for the shot noise and the thermal noise envelopes at the output terminal, where sinusoidal LO signal, $v_{LO}(t) = V_{LO} \cos \omega_{LO} t$, is applied to the BHMIX.

Fourier coefficients c_n of envelope functions were calculated for (26) and (29), by numerically integrating (A·6). Then $|c_n|^2$ was accumulated until relative error of the sum became less than 10^{-5}. For example, the sum was taken up to $n = 50$ for $V_{LO} = 1$ V. Smaller V_{LO} values need much less terms. Here, $\beta_F = 100$ was assumed for shot noise calculation. Note that $\sum |c_n|^2$ values scale with I_Q, r_b and β_F, so that we need not recalculate them under various bias conditions.

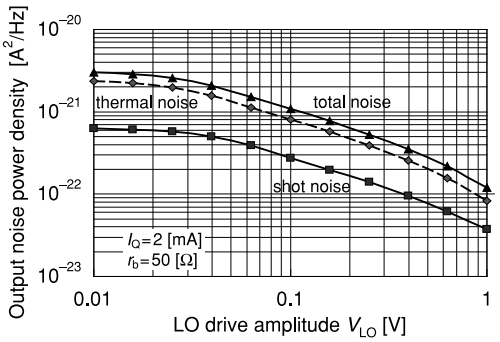

Fig. 9 Output noise power densities versus LO drive amplitude. Calculated for $I_Q = 2$ mA, and $r_b = 50\,\Omega$.

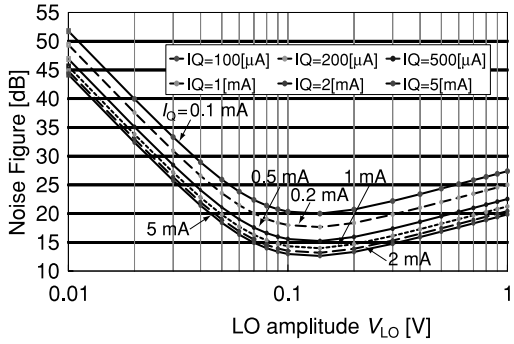

Fig. 10 Calculated relation between noise figure and LO amplitude for various I_Q ($r_b = 50\,\Omega$).

Reference [6] calculated only $|c_0|$ for shot noise component, while $\sum |c_n|^2$ was calculated for thermal noise of r_b. Thus it may underestimate the total noise power.

Figure 9 shows an example of the result under a realistic condition; i.e, I_Q=2 mA and $r_b = 50\,\Omega$. Thermal noise component dominates over shot noise component in the total noise power under this condition.

3.6 Equivalent Input Noise and Noise Figure

Equivalent input rms noise V_{neq} can be calculated by converting the total output noise back into the RF input terminal voltage by using the normalized conversion gain η. Considering the normalizing factors, we have

$$V_{neq} = \frac{1}{\eta} \frac{2V_T}{\alpha_F I_Q} I_{ntotal}, \tag{32}$$

where I_{ntotal} stands for the total output rms noise current.

Once the equivalent input noise V_{neq} is calculated, this noise source resides in series with the base terminal at the input of the BHMIX; thus V_{neq} can be directly compared with a thermal noise voltage of the signal source impedance R_S. Hence noise figure, NF, can readily be calculated by the following equation:

$$\mathrm{NF} = 10 \log \left\{1 + V_{neq}^2/(4kTR_S)\right\}. \tag{33}$$

Figure 10 shows some calculated NF curves for various I_Q values. This clearly indicates that the minimum

NF occurs around $V_{LO} = 0.15$ V. These were calculated for $r_b = 50\,\Omega$, where shot noise component dominates in $I_Q = 100\ \mu$A, and thermal noise component dominates in $I_Q > 1$ mA cases. Therefore, LO amplitude of $V_{LO} = 0.15$ V is concluded to be the optimal operating point from NF point of view.

From Fig. 10, we see that NF improvement saturates with I_Q. Therefore, practical limit of I_Q may be around several milliamperes, considering power dissipation.

It should be noted that the proposed NF calculation method can be directly applicable to the Gilbert type mixer by simply changing the input noise reference point.

4. Comparison with Measured Results

The analysis results are compared with measured data, which are taken from references [2] and [3]. The BHMIX circuit schematic is shown in Fig. 11, where an input impedance for LO port is 25 Ω (single ended), and RF port impedance is 50 Ω (balanced). Estimated parameter values $I_Q = 2$ mA and $r_b = 50\,\Omega$ are used for theoretical calculations in this section.

It should be noted that the measured circuit is a single-balance version of the simple BHMIX, so that the input RF level is halved for each unit BHMIX.

4.1 Conversion Gain

Measured conversion gain plot against LO amplitude is shown in Fig. 12. This matches well with Fig. 2. The largest conversion gain occurs at about −8 dBm for 25 Ω, which corresponds to 89 mV (peak value) and this is close to the predicted value of 100 mV. Note that we actually obtained conversion *gain* instead of loss in this case.

4.2 Self-Mixing

The self-mixing induced output dc offset is hardly distinguished from other sources of dc offsets; therefore, an 1.00005 GHz simulated LO signal was input to the RF port in place of an LO leakage, while an 1.00000 GHz LO signal being input to the LO port. The result is shown in Fig. 13 by "□" symbols along with input-referred noise level [2].

It is observed from the figure that the equivalent input level at RF port, $V_{self-mixing}$, rises in proportion to the simulated LO signal level above about −5 dBm, as expected from the discussion on Fig. 5. However, a total amount of equivalent input offset could not be estimated since it depends on a degree of matching between the two unit BHMIXs, of which we don't have information.

Below about −10 dBm, the equivalent input level at the RF port stays almost constant at about −97 dBm. This residual component could be attributed to imbalances other than offset, but the source has not been identified.

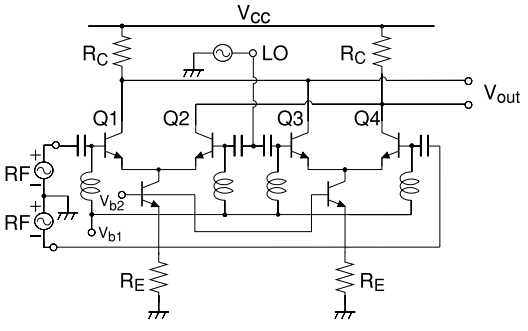

Fig. 11 Test chip circuit of single balance BHMIX [2].

4.3 Second-Order Intercept Point

The IIP2 value of over +37 dBm has been reported in [3]. This value is believed to be dominated by the offset of differential pairs, which can be consistent with the discussion in section 2.3, where IIP2=+34.2 dB is predicted for $V_{OS} = 0.52$ mV. Even so, there found some chips with IIP2 ≈ +50 dBm as shown in Fig. 14.

4.4 Third-Order Intercept Point

Figure 14 shows a measured dependence of fundamental output and IM3 output on RF-signal level [2]. From this plot, we have IIP3=−1 dBm for LO signal of −6 dBm for 25 Ω ($\alpha \approx 2.1$). As we obtained IIP3 ≈ −9.0 dBm by using the result of Fig. 3, the predicted IIP3 for this case becomes

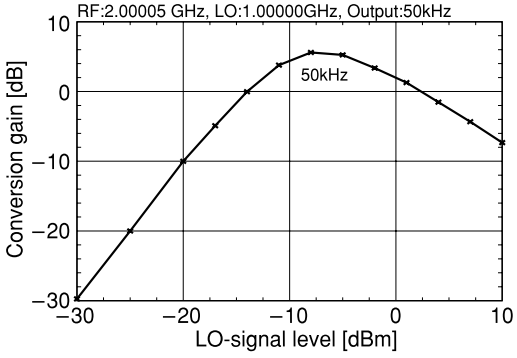

Fig. 12 Dependence of conversion gain on LO-signal level (measured).

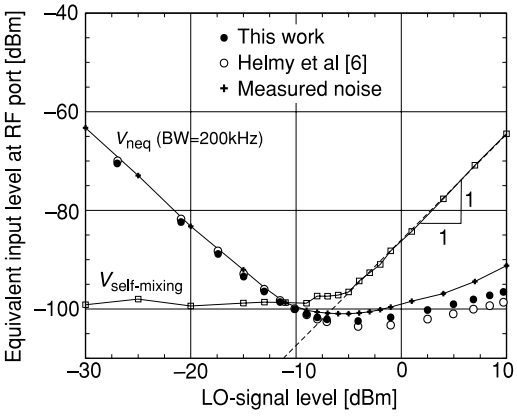

Fig. 13 LO-signal level vs. equivalent input level at RF port (measured).

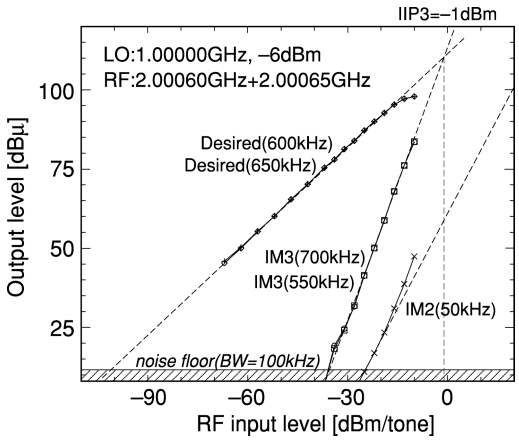

Fig. 14 Dependence of IM3 and IM2 on RF-signal level (measured).

about −3 dBm, considering the correction of 6 dB improvement due to the balanced structure. This is close to the measured value.

4.5 Equivalent Input Noise

The RF input of the test chip is divided in two and down-converted by two identical BHMIXs, and the outputs are combined into one at the output. Thus, the NF value must remain the same for a single BHMIX.

The measured noise data are plotted with "+" symbols in Fig. 13. The calculated equivalent input noise voltage by our method is overlaid on it with "•" symbols. Also, calculated V_{neq} by the method of [6] is plotted on it with "○" symbols. Measured and calculated results fit fairly well, but our method fits better. As it is predicted, method in [6] gives 2 to 4 dB lower estimate because it excludes the folding effect in shot noise calculation for large LO amplitude. Both methods match the measured results very well for low LO signal level region. This is because the thermal noise dominates in this region for $I_{\mathrm{Q}} = 2$ mA.

It should be noted that our proposed analysis method agreed very well with the measured data at a very high frequency, 2 GHz, even though it covers only static nonlinearity.

5. Conclusion

Nonlinear large-signal analysis of a bipolar harmonic mixer (BHMIX) and its verification using test chips are presented in this paper. Analytical expressions for conversion gain, IIP3, IIP2, and self-mixing induced dc-offset, NF are obtained and numerical results are shown.

From the results of the analysis, it was estimated that the variation of self-mixing induced dc-offset in the balanced BHMIX can be as small as −100 dBm under practical conditions. This was confirmed by a test chip measurement.

The predicted characteristics by nonlinear large-signal analysis are compared with measured results and we obtained a good correlation between the analysis and the measured results.

Also, a noise analysis method is proposed for BHMIX. Both thermal noise and shot noise are modeled as amplitude modulated white noises, which are treated as cyclostationary noises. The analysis includes all the folding noises from high frequencies. The total output noise can be calculated by weighting and summing two universal output noise curves, namely $\sum |c_n|^2$ as a function of V_{LO} for shot noise and thermal noise, once tail current I_{Q} and base resistance r_{b} are given. The measured noise and calculated noise agree very well even though the method covers only static nonlinearity. The optimal LO signal drive amplitude is determined to be about 0.15 volts. It has been clarified that the thermal noise of base resistance dominates over shot noise under typical operation conditions.

In conclusion, we can predict critical performances of a BHMIX before going into a detailed circuit design by using the analysis results.

Acknowledgment

The authors would like to thank Kazuya Matsuhira of DNP LSI Design Co. Ltd., for useful discussion on noise analysis of differential pair. They are also deeply indebted to Prof. Hideaki Sakai of Kyoto University for his kind guidance in cyclostationary noise analysis.

References

[1] A.A. Abidi, "Low-power radio-frequency IC's for portable communication," Proc. IEEE, vol.83, no.4, April 1995.
[2] T. Yamaji and H. Tanimoto, "A 2 GHz balanced harmonic mixer for direct-conversion receivers," IEEE 1997 Custom Integrated Circuits Conference, 9.6, pp.193–196, May 1997.
[3] T. Yamaji, H. Tanimoto, and H. Kokatsu, "An I/Q active balanced harmonic mixer with IM2 cancelers and a 45 phase shifter," IEEE J. Solid-State Circuits, vol.33, no.12, pp.2240–2246, Dec. 1998.
[4] H. Yoshida, T. Toyoda, I. Seto, R. Fujimoto, O. Watanabe, T. Arai, T. Itakura, and H. Tsurumi, "Fully differential direct-conversion receiver for W-CDMA reducing DC-offset variation," IEICE Trans. Electron., vol.E87-C, no.6, pp.901–908, June 2004.
[5] H. Tanimoto and T. Yamaji, "A balanced harmonic mixer based on BJT differential pairs," 2001 Microwave Workshop and Exhibition (MWE'01), WS11-03, Dec. 2001.
[6] A. Helmy, K. Sharaf, and H. Ragai, "Analysis and optimization of noise in bipolar RF harmonic mixers," Analog Integr. Circuits Signal Process., vol.37, no.3, pp.139–148, Dec. 2003.
[7] H. Tanimoto and R. Ito, "Noise analysis of bipolar harmonic mixer," 2004 47th Midwest Symposium on Circuits and Systems, pp.III-359–III-362, July 2004.
[8] M. Cohn, J.E. Degenford, and B.A. Newman, "Harmonic mixing with an antiparallel diode pair," IEEE Trans. Microw. Theory Tech., vol.MTT-23, no.8, pp.667–673, Aug. 1975.
[9] K. Itoh, K. Kawakami, M. Shimozawa, N. Suematsu, and A. Iida, "Even order mixing products of even harmonic mixer for direct converter," Proc. IEICE General Conf., vol.4, C-87, March 1995.
[10] B. Razavi, RF microelectronics, Chapt. 2, Prentice Hall PTR, Nov. 1997.
[11] H. Tanimoto, "Mission impossible? A review of mixers for direct-conversion receivers," IEICE Trans. Electron. (Japanese Edition), vol.J84-C, no.5, pp.337–348, May 2001.
[12] M. Okumura, H. Tanimoto, T. Itakura, and T. Sugawara, "Numerical noise analysis for nonlinear circuits with a periodic large signal ex-

citation including cyclostationary noise sources," IEEE Trans. Circuits Syst. I, Fundam. Theory Appl., vol.40, no.9, pp.581–589, Sept. 1993.

[13] W.A. Gardner, Introduction to random processes: with applications to signals and systems, 2nd ed., Chapt. 12, McGraw-Hill, New York, 1989.

[14] K.L. Fong and R.G. Meyer, "Monolithic RF active mixer design," IEEE Trans. Circuits Syst. II, Analog Digit. Signal Process., vol.46, no.3, pp.231–239, March 1999.

Appendix: Power Spectrum Density of a Periodically Amplitude Modulated White Noise

An amplitude modulated white noise $n(t)$ can be modeled by (24), and such $n(t)$ becomes a cyclostationary process with a period T [13]. We assume $E[n(t)] = 0$ for simplicity, where $E[\cdot]$ stands for *an expectation of*. Then the auto-covariance of $n(t)$, i.e, $R_n(t+\tau, t) = E[n(t+\tau)n(t)^*]$, is also T-periodic and can be expanded into a Fourier series:

$$R_n(t+\tau, t) = \sum_{k=-\infty}^{+\infty} C_k(\tau)\, \mathrm{e}^{\mathrm{j}\frac{2\pi k}{T}t}, \quad \text{with} \tag{A·1}$$

$$C_k(\tau) = \frac{1}{T}\int_{-T/2}^{T/2} R_n(t+\tau, t)\, \mathrm{e}^{-\mathrm{j}\frac{2\pi k}{T}t}\, \mathrm{d}t, \tag{A·2}$$

where $C_k(\tau)$ is a k-th Fourier coefficient. Now, $C_k(\tau)$ can be expressed by Fourier transform:

$$C_k(\tau) = \frac{1}{2\pi}\int_{-\infty}^{+\infty} S_k(\omega)\mathrm{e}^{\mathrm{j}\omega t}\, \mathrm{d}\omega, \quad \text{with} \tag{A·3}$$

$$S_k(\omega) = \int_{-\infty}^{+\infty} C_k(\tau)\mathrm{e}^{-\mathrm{j}\omega\tau}\, \mathrm{d}\tau. \tag{A·4}$$

Note that $S_0(\omega)$ is a time-averaged spectrum density of $n(t)$, which is to be measured by an ordinary instrument like a spectrum analyzer.

For (24) we have the covariance function:

$$R_n(t+\tau, t) = a(t+\tau)a^*(t) \cdot R_w(\tau), \tag{A·5}$$

where $R_w(\tau)$ is an autocorrelation function of the stationary noise $w(t)$. As $a(t)$ is a periodic function,

$$a(t) = \sum_{m=-\infty}^{+\infty} c_m \mathrm{e}^{\mathrm{j}\frac{2\pi m}{T}t}, \quad \text{with} \quad c_m = \frac{1}{T}\int_{-T/2}^{T/2} a(t)\, \mathrm{e}^{-\mathrm{j}\frac{2\pi m}{T}t}\, \mathrm{d}t \tag{A·6}$$

holds. Putting (A·5) and (A·6) into (A·3) and (A·4), we have a Fourier expansion pair:

$$C_k(\tau) = \sum_{n=-\infty}^{+\infty} c_{n+k}c_n^* \mathrm{e}^{\mathrm{j}\frac{2\pi(n+k)}{T}\tau} R_w(\tau), \tag{A·7}$$

$$S_k(\omega) = \sum_{n=-\infty}^{+\infty} c_{n+k}c_n^* S_w\left(\omega - \frac{2\pi(n+k)}{T}\right), \tag{A·8}$$

where $S_w(\omega)$ is a power spectrum density of $w(t)$.

If we use a spectrum analyzer to measure the power spectrum density of $n(t)$, it must be a time-averaged power spectrum $S_0(\omega)$, and hence we have

$$S_0(\omega) = \sum_{n=-\infty}^{+\infty} |c_n|^2 S_w\left(\omega - \frac{2\pi n}{T}\right) \approx \sigma^2 \sum_{n=-\infty}^{+\infty} |c_n|^2, \tag{A·9}$$

on the condition that the Fourier coefficients $|c_n|$ decrease rapidly with n, as is the usual case. Here, $\sigma^2 = S_w(\omega)$ is a power spectrum density of the white noise $w(t)$. In conclusion, therefore, measured power spectrum density is constant, and is a product of the white noise power spectrum density and the power of the modulating function.

Hiroshi Tanimoto was born in Hokkaido, Japan, in 1953. He received the B.E., M.E., and Ph.D. degrees in Electronic Eng. from Hokkaido University, in 1975, 1977, and 1980, respectively. In 1980 he joined the Research & Development Center, Toshiba Corp., Kawasaki, Japan, where he was engaged in research and development of telecommunication LSIs. Since 2000, he has been a Professor in the Dept. of Electrical and Electronics Eng., Kitami Institute of Technology, Kitami, Japan. His main research interests include analog integrated circuit design, analog signal processing, and circuit simulation algorithms. Dr. Tanimoto is a member of IEEJ and IEEE.

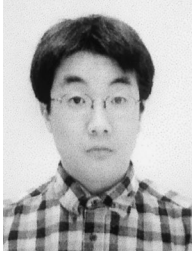

Ryuta Ito was born in Hokkaido, Japan, in 1981. He received the B.E. degree in Electrical and Electronic Eng. from Kitami Institute of Technology, Kitami, Japan, in 2004. He is currently a graduate student at Kitami Institute of Technology, and studying noise analysis of mixer circuits.

Takafumi Yamaji was born in Fukuoka, Japan, in 1965. He received the B.E., M.E., and Ph.D. degrees in Communication Eng. from Kyushu University, Fukuoka, Japan, in 1988, 1990, and 2004, respectively. In 1990 he joined the Research & Development Center, Toshiba Corp., Kawasaki, Japan. Since then he has been engaged in the research and development of wireless communication circuits. His present field of interest is signal processing for communication.